JFLS 20000355 PROD.TYPE: COM
pp. 1–12 (col.fig.: NIL)
ED: Gracy
PAGN: ANG – SCAN: Raghavendra

Journal of Fluids and Structures (2001) **15,** 000–000
doi:10.1006/jfls.2000.0355, available online at http://www.idealibrary.com on IDEAL

ENERGY HARVESTING EEL

J. J. Allen and A. J. Smits

Department of Mechanical and Aerospace Engineering, Princeton University
Princeton, NJ 08543, U.S.A

(Received 1 September 2000, and in final form 16 November 2000)

The current study examines the feasibility of placing a piezoelectric membrane or "eel" in the wake of a bluff body and using the von Kármán vortex street forming behind the bluff body to induce oscillations in the membrane. The oscillations result in a capacitive buildup in the membrane that provides a voltage source that can be used, for example, to trickle-charge a battery in a remote location. The aim of the hydrodynamic testing is to maximize the strain energy and mechanical power by coupling the unsteady flow field with the vibration of the membrane. The requirement of optimal coupling is best defined as a resonance condition where the membrane has a negligible damping effect on the original von Kármán vortex street.

1. INTRODUCTION

Literature related to the characteristics of bluff body wakes is extensive and there is also considerable literature related to the problem of flutter and the response of flexible structures placed in a cross-flow. The response of a flexible membrane may be considered to demonstrate aspects of these phenomena. Flows behind bluff bodies in the Reynolds number range 10^3–10^5 are characterized by the formation of a vortex street of reasonably constant Strouhal number with respect to Reynolds number. The vortex streets in this range have a strongly three-dimensional character. Huerre & Monkewitz (1990) provide a description and review the formation of the von Kármán street in terms of being the result of a local absolute instability growing into a global linear instability, and arguing against the mechanism if the vortex street formation does not involve details of flow separation. The presence of a rigid splitter plate behind a bluff body can have dramatic effects in terms of reducing and suppressing vortex street formation and therefore the stability characteristics of the flow, e.g., Roshko (1954), Gerrard (1966). These studies highlighted the way the presence of a splitter plate of increasing length can delay and eventually prevent the formation of oscillations in the wake. The effect of splitter plates is relevant in the current study as in some flow configurations the membrane is stiff enough to have the effect of a rigid splitter plate. If the membrane has small inertia and is flexible enough to be able to respond rapidly to the unsteady pressure field set up by the vortex shedding, one may expect that the membrane may oscillate with a wavelength and frequency similar to that observed in the unobstructed wake. This results in a coupled fluid/structure problem.

The study of oscillating structures by flow fields is often described in terms of free and forced vibration. If one considers a simplified description of the displacement of the structure in the spanwise direction, $y(x, t)$, as a mechanical system of mass m subject to an external force field, then

$$m\ddot{y}(t, x) + H(\dot{y}, y, x, t) = f_1 + f_2. \tag{1}$$

0889–9746/01/070593 + 20 $35.00/0

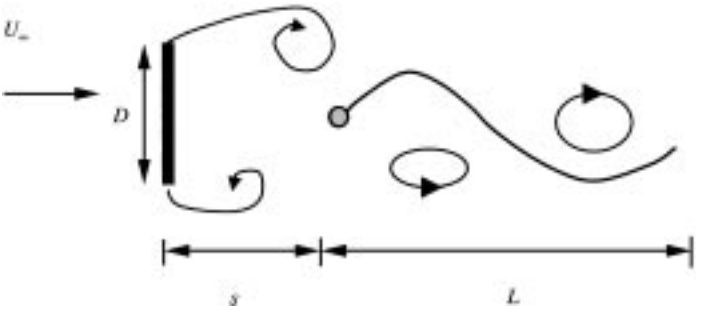

Figure 1. Geometry of oscillating membrane behind a flat plate.

The function H represents internal restoring forces related to the body stiffness and damping properties. The forcing function on the right-hand side, which is the result of the external flow field, is often expressed as the sum of two parts. The first term f_1 is the free vibration forcing field and represents the self-induced effects of the unsteady wake, generated by vortex shedding. This type of excitation has been classified as movement-induced excitation (MIE); see, e.g., Naudascher & Rockwell (1994), Khalak & Williamson (1999). This type of forcing is the mechanism responsible for wing flutter.

The second term, f_2, represents the effect of an external forcing field that has its source remote from the body being excited. This type of forcing is classified as extraneously induced excitation (EIE) and is a feature of "gusting". Paidoussis (1966*a*) developed relationships for the stability of a long flexible slender cylinder, orientated parallel with the free stream. He developed an approximation for the unsteady pressure field acting on the cylinder by using small-amplitude assumptions and an approximation for the added mass of the cylinder when oscillating in the free stream. Using this expression for the pressure differential based on the shape and velocity of the cylinder, the conditions of stability for the successive modal shapes based on cylinder properties and flow conditions were calculated. The flow-induced oscillations were self-excited and the experiments of Paidoussis (1966*b*) showed oscillation dominated by single modes. In contrast, we are interested in the excitation of a membrane produced by the vortex shedding of the bluff body.

2. EXPERIMENTS

A number of different membranes were tested in a water channel running at speeds of 0·05–0·8 m/s. Two different bluff body sizes were used, 5·08 and 3·81 cm, resulting in a Reynolds number range, $\mathrm{Re}_D = U_\infty D/v$, of 5×10^3–4×10^4. The aspect ratios of the bluff bodies were 6 and 10, respectively.

Figure 1 shows the important experimental parameters involved in describing the behavior of the undulating eel, D is the width of the bluff body, s is the distance downstream of the bluff body where the head of the eel is placed, and U_∞ is the free-stream velocity. The physical properties of the eel are described in terms of its stiffness E, length L, thickness h, width W and mass per unit length ρ_{eel}. Figure 1 also shows an interpretation of the type of vortical structures forming over the membrane.

Experiments were conducted in a recirculating water channel 18 in wide and 5 in deep (1 in = 25·4 mm). The ratio of gap width to bluff body size was equal to unity in the current experiments and not varied. Flow visualization using fluorescent dye and particle image velocimetry (PIV) experiments both used a laser sheet generated from a continuous 7 W argon-ion laser to take a cross-section through a horizontal plane of the flow.

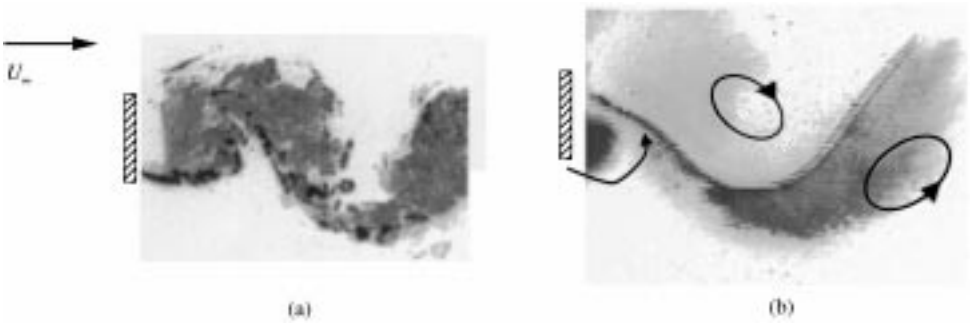

Figure 2. (a) Formation of von Kármán vortex street without membrane and (b) the formation of a coherent wake behind the bluff body with a flexible membrane present.

Figure 2(a, b) shows dye visualization images behind a 5·08 cm bluff body with and without an eel present at $\mathrm{Re}_D = 10\,000$. At this Reynolds number, the vortex shedding behind the plate, although coherent, is strongly turbulent and three dimensional. The membrane in this case is executing large forced oscillations, and the conjectured vortical structures are highlighted in Figure 2(b). The spacing of vortical structures in both cases is of the order $1.9D$. Although the flow visualizations in Figure 2 show a somewhat similar spacing of structures, the overall topologies of the two flows must be different, as the membrane acts as a streamline to prevent communication between the separating shear layers.

The PIV system consists of an externally triggered Cohu 6600–3000 series full frame transfer camera, 659×496 pixels, with 10-bit resolution. The acquisition timing sequence is as follows. The first frame is triggered for a short electronic exposure, of the order of 1 ms in the current experiments. The transfer time for the first frame is 17 ms. While the data for the first image are being transferred, the camera is triggered for a second exposure. The exposure period for the second image is set electronically for 17 ms, the maximum time exposure for a single frame. However, rather than expose the CCD array to the laser light for this period, the light source is interrupted mechanically in order to have an equivalent exposure time in the second frame as in the first. This system allows an effective Δt between images of the order 0·5 ms if required and an image pair acquisition rate up to 30 Hz. It is critical for the electronic exposure period in the second image to be 17 ms, as this prevents corruption of the data transfer of the first image, i.e., all the data from the first image have been transferred before the second image data transfer begins.

To generate information on the unsteady shape of the eel, a series of images were grabbed to PC RAM at a rate of 60 Hz. Figure 3(a) shows superimposed images of the oscillating eel over a full cycle, which is used to define a maximum amplitude. The instantaneous membrane images were interrogated with edge detection software to extract information about the instantaneous position of the membrane. Figure 3(b) shows a sequence of membrane shapes after edge processing, superimposed on the one plot.

In the Reynolds number range 5000–50 000 the Strouhal number, St, behind the 1·5 in bluff body was equal to $0{\cdot}155 \pm 0{\cdot}002$, and for the 2 in bluff body it was $0{\cdot}160 \pm 0{\cdot}002$. This slight variation is a function of increased tunnel blockage. The Strouhal number was essentially invariant over the range of Reynolds numbers being investigated. Four membranes were tested. The first two were 18 in and 24 in long, made from polyvinyline di-floride (PVDF), which is a piezoelectric material that when strained generates a voltage potential in capacitor-like polymers. A third membrane was made primarily from polyurethane (PU), with two thin outer layers of PVDF attached to the polyurethane. The

(a) (b)

Figure 3. (a) Superposition of membrane shapes and (b) a sequence of individual membrane shapes.

TABLE 1
Properties of membranes tested

	Thickness, t (mm)	Length, L (m)	Mass, m (g)	EI/ρ_{eel} ($m^4 s^{-2}$)	L/D (—)
18 in PVDF eel	0·7	0·457	38	0·0028	12, 18
24 in PVDF eel	0·7	0·076	53	0·0028	12
18 in PU eel	0·6	0·457	34	0·00062	12
18 in Plastic eel	0·1	0·457	7	0·0021	12

fourth membrane was made from plastic shim stock, selected so as to have similar natural frequencies to the 18 in PVDF membrane but with a much smaller mass per unit length. The width of all membranes, W, was 0·0762 m.

The properties of the eels tested are listed in Table 1. Here I is the moment of area and ρ_{eel} is the mass per unit length of the eel. The term EI/ρ_{eel} represents the effective stiffness of the eel in response to bending, and its value was determined directly from a deflection test. This term is somewhat similar to the spring–mass ratio which is used to describe the undamped natural frequency of a spring–mass system.

The internal damping of the shim-stock eel is a factor of approximately two smaller than the PVDF and PU, as estimated from a free vibration experiment in air. Values of length of the eel to the bluff body size, L/D, are also shown. To assess the behavior of this range of eels, measurements were made of the frequency of oscillation and amplitude, as defined in Figure 3(a). Figure 4(a) shows the ratio of the response frequency f_{eel} to the natural frequency f_{nat} with increasing Re_D, and Figure 4(b) shows the ratio of eel amplitude to bluff body with increasing Re_D for the PU membrane.

At Reynolds number of order 1000, the amplitude of oscillation of the membrane is small and the ratio of frequencies is about 0·5. The oscillation in this case is infrequent. In this mode, the behavior of the eel can be interpreted as being similar to that of a rigid splitter plate. At Reynolds numbers less than 500, the eels appear to be causing the separated shear layers from the bluff body to reattach on the eel surface and form an essentially closed recirculation bubble on the eel, as shown in the dye visualization image in Figure 5.

At a Reynolds number of order 10 000, the membrane begins to oscillate at a fairly constant frequency. An image of the membrane flapping in this mode is shown in Figure 6(a). Although the membrane appears to be oscillating with an apparently traveling waveform, it is not well coupled to the flow, as indicated by the fairly low value of $f_{eel}/f_{nat} \approx 0{\cdot}6$–$0{\cdot}8$, indicating that the membrane exerts a damping effect on the flow. As the Reynolds number is further increased, the eel gradually shortens in length. This results in

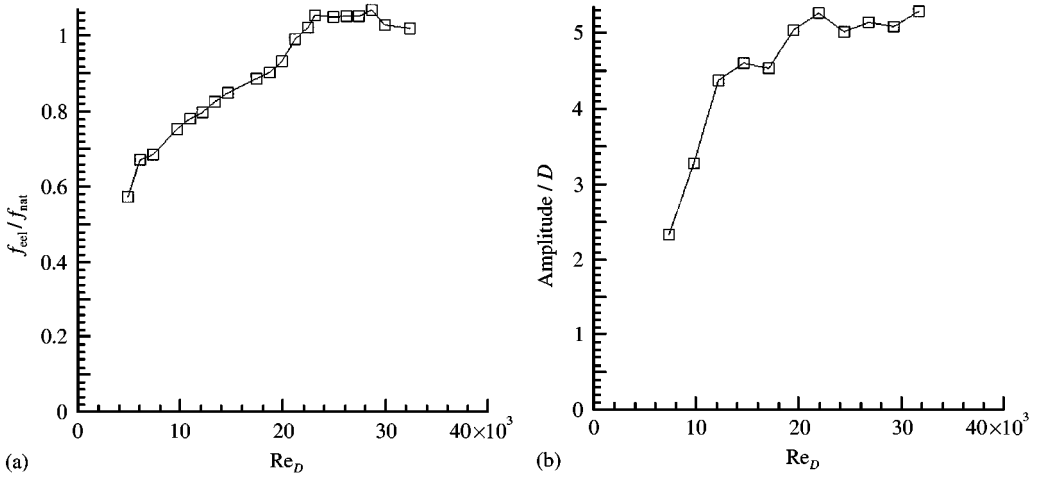

Figure 4. (a) Plot of frequency response and (b) amplitude of the PU membrane versus Reynolds number.

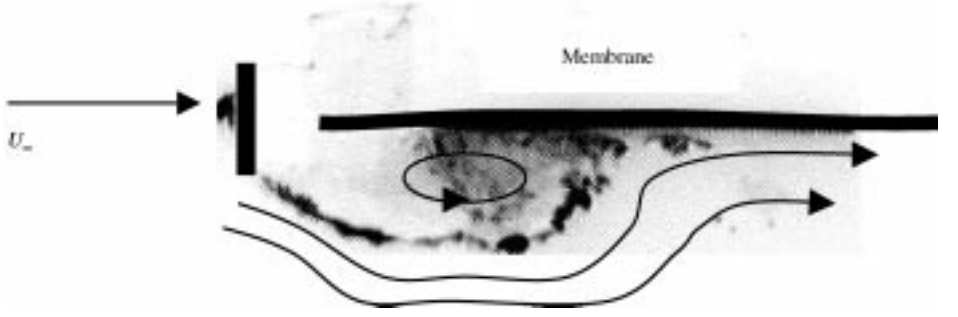

Figure 5. Flow visualization of PU membrane at $Re_D = 1000$.

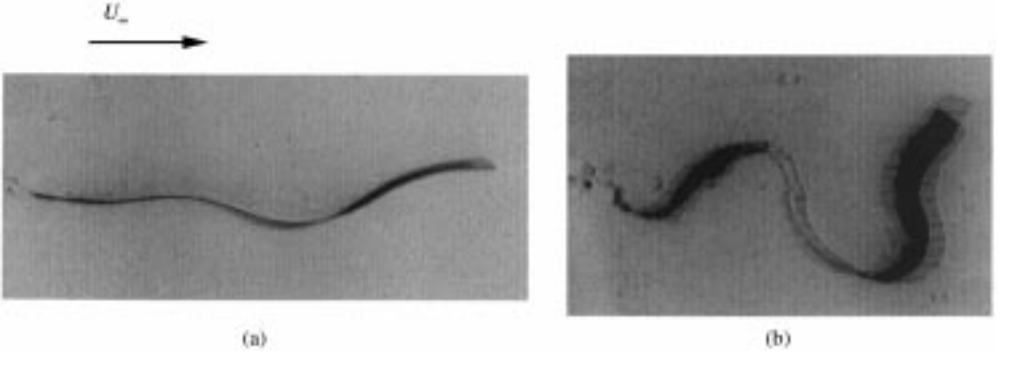

Figure 6. Membrane oscillation: (a) $Re_D = 10\,000$; (b) $Re_D = 20\,000$.

a decrease in wavelength and an increase in amplitude of oscillation. As this occurs, there is also a trend for the frequency ratio to approach unity, indicating that the eel is well coupled to the flow. The wavelength of the membrane shortens to a point where it appears that it closely resembles the wavelength of the coherent structures in the wake of a plate without

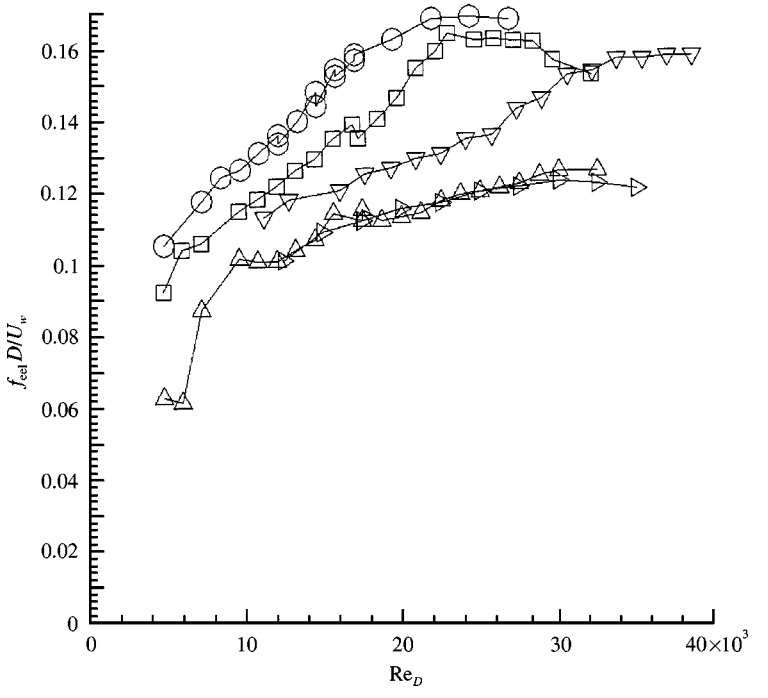

Figure 7. Scaling of Strouhal number versus Reynolds number for a range of membranes: □, ρU; △, 18 in PVDF, $D = 1{\cdot}5$ in; ▽, 24 in PVDF, $D = 2{\cdot}0$ in; ▷, 24 in PVDF, $D = 1{\cdot}5$ in; ○, 101 μ in shim stock.

a membrane being present, as shown in Figure 6(b). The amplitude of oscillation of the membrane in Figure 6(b) appears to be similar or larger than the width of the wake when the membrane is not present. This would indicate an increased momentum deficit caused by the motion of the membrane.

As the Reynolds number increases beyond $2{\cdot}0 \times 10^4$ for the membrane shown in Figure 6 we see relatively constant amplitude of oscillation and a linear increase of frequency of oscillation with flow velocity. The concatenation of the wavelength of the eel translates directly into an increase of amplitude, which seems to indicate the length of the eel is essentially constant. The amplitude of response and the frequency ratio f_{eel}/f_{nat} appear to be directly related, as the amplitude plots versus Re_D show similar trends. Note that when the eel reaches the optimal coupling condition and its effective wavelength is fixed, and if it is not being stretched, the amplitude will remain constant. This apparent length preserving aspect of eel behavior also suggests that tension is not an important factor when considering the dynamics of the eel. It also implies that the phase speed of structures convecting along the eel surface is approximately constant for a fixed flow velocity, regardless of the ability of the eel to couple to the flow. The phase speed is defined as $U_{phase} = \lambda f_{eel}$. The fact that the eel amplitude appears to reach a maximum may indicate the effect of the free stream or internal damping. The membrane appears to be able to oscillate with a maximum amplitude that is similar to the natural wake width, but does not exceed it, despite being forced close to its natural frequency.

Figure 7 shows the response of the range of eels tested, plotted with respect to their nondimensional frequency, $f_{eel}D/U_\infty$ and bluff body Reynolds number, Re_D.

The various data sets show that, as the Reynolds number increases, the trend of the membrane behavior is towards optimal flow coupling, defined by $f_{eel}D/U_\infty \approx 0.16$, which is

equivalent to $f_{eel}/f_{nat} \approx 1$. This trend can be seen in all the data sets as the flow speed increases, suggesting that there may be a similarity scaling to describe the membrane behavior. However, the different membranes approach $f_{eel}/f_{nat} \approx 1$ at different rates when scaled with respect to Reynolds number. This can be explained by the fact that the Reynolds number does not take into account any material properties of the eel, which obviously have a significant effect on the membrane response. Important aspects of the above data sets are that the frequency response of the 24 in and 18 in eel behind the 1·5 in plate are identical, suggesting that the membrane response does not depend critically on the length of the membrane, at least for the relatively large L/D ratios we are considering here. The 24 in eel displays a marked improvement in response behind the 2 in bluff body, compared to the 18 in eel placed behind the 1·5 in bluff body, indicating a significant response sensitivity to the bluff body size. The shim-stock eel, which has almost the same natural frequencies as the 18 in PVDF eel displays far superior coupling to the flow, suggesting that an inertial or internal damping factor is important to describe the membrane behavior. The data sets show a leveling out of the nondimensional frequency, indicating that the oscillation appears to have an upper bound of frequency as determined by the bluff body size and flow speed. This would also seem to indicate that the observed phenomenon is not a self-excited, but is critically dependent on the presence of the bluff body.

3. NONDIMENSIONAL DESCRIPTION OF MEMBRANE BEHAVIOR

A simplified description of the motion of the membrane, $y(x, t)$, is given by the Euler–Bernoulli beam equation where the forcing function $f(x, t)$ is the effect of the fluid on the membrane:

$$\frac{d^2y}{dt^2} + \frac{\zeta}{\rho_{eel}}\frac{dy}{dt} + \frac{EI}{\rho_{eel}}\frac{d^4y}{dx^4} - T\frac{d^2y}{dx^2} = f(x, t). \tag{2}$$

The solution for the displacement of the membrane can be represented as $y(x, t) = \sum_{n=1}^{\infty} \Phi_n(x) A_n(t)$, where $\Phi_n(x)$ represent an orthogonal set of eigenfunctions. These eigenmodes were used by Paidoussis (1966*a*) to describe the dynamics of a flexible cylinder, pinned at both ends, in a stream. For the case of the cylinder pinned at one end and free at the other Paidoussis (1966*a*) used a power-series expansion for the shape of the cylinder. Wu (1961), in contrast, used traveling waves to describe the motion of a swimming plate through water. The choice of the orthogonal basis functions in the current study is based on the approximation of the membrane with an Euler–Bernoulli beam and provides a compact, though not necessarily unique way to describe the membrane motion. If we neglect the effects of tension and damping, this equation also yields information on the natural frequencies of these modes, which may be expressed as $\omega_n = (\beta_n^2/l^2)\sqrt{EI/\rho_{eel}}$, where β_n represent the eigenvalues corresponding to $\Phi_n(x)$, which depend on the boundary conditions of the membrane. If single-mode excitation were to be possible, it would imply that the membrane is oscillating as a standing wave. This would mean a significant departure of the flow field topology from the natural von Kármán street, which seems unlikely as the mass ratio is small, $\rho_{eel}/\rho \approx 1{\cdot}3$, and hence, we expect a broadband response of the membrane. If the membrane is to follow closely the forcing of the von Kármán street, as experiments show, then the forcing is essentially a traveling pressure wave. Since the membrane is fixed at a pivot point, the only way its response can resemble a traveling wave is if there are significant contributions to the eel shape from more than one mode.

Data sets for the shape of the eel have been projected onto the eigenmodes to evaluate the contribution of each mode to the shape of the eel. Figure 8(a) shows the relative modal contributions $A_n(t)$, varying in time, for modes 0–5 for the PU eel operating at 0·36 m/s

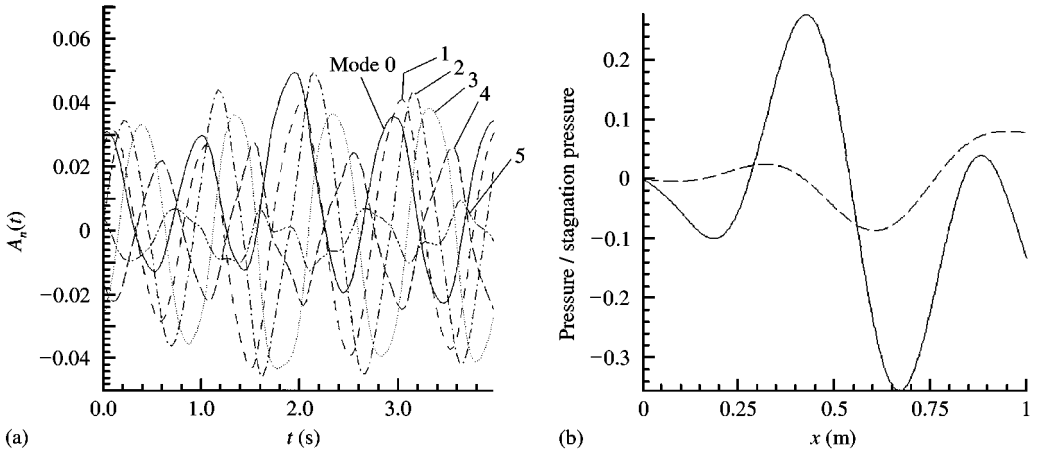

Figure 8. (a) Modal contributions to shape of membrane ———, mode 0; – – –, mode 1; —.—., mode 2; ....., mode 3; — — —, mode 4; –..–..–, mode 5 and (b) pressure field acting across membrane. In (b): ——, pressure/stagnation pressure; – – –, eel.

behind a 1·5 in bluff body. The modal contributions start to decay significantly past mode 4 and hence we have a fairly compact data set to describe the eel motion. The functions $A_n(t)$ oscillate at the same frequency and display significant phase differences between successive modes. The fact that we have multiple modes present rather than a dominant single mode, coupled with the earlier observation that the peak frequency ratio $f_{\text{eel}}/f_{\text{nat}} \approx 1$ seems to be linked directly to the size of the bluff body, would seem to indicate that the motion of the membrane is not self-excited. Substituting the experimental data for $y(x, t)$ into the linearized equation of motion [equation (2)] and neglecting the effects of damping and tension, yields an expression for the pressure field acting on the eel. Figure 8(b) shows a plot of the pressure differential, normalized with respect to the stagnation pressure, $\frac{1}{2}U_\infty^2\rho$, acting across the eel. The pressure differential is a small fraction of the stagnation pressure, which seems to indicate that the reduced differential equation description of the system is reasonable. An accurate test of this assumption would be from a PIV measurement of the velocity differential across the membrane. The pressure differential at the tail of the eel indicates that a velocity difference exists at this point and hence the possibility exists of measuring vortex shedding into the wake. Figure 8(b) indicates that the wavelength of the forcing function is similar in shape to the eel and hence similar in shape to the pressure field set up by a traveling vortex street. This suggests that the forcing is related in frequency to the size of the bluff body, and hence the Strouhal number. An example of the reconstructed shape of the membrane using the first 5 modes is also shown in Figure 8(b).

If the form of the forcing function is modeled as a traveling wave, it may be approximated by $P(x)\sin(2\pi/\lambda(x - ct))$ where λ is the wavelength of the disturbance given by the von Kármán vortex street; so that $c \approx \lambda U_\infty \text{St}/D$. The magnitude of the forcing will be a fraction of the stagnation pressure. From experimental data this function is of the order of $P(x) \approx 0{\cdot}1\rho D U_\infty^2 W/\rho_{\text{eel}}$. Projection of the eigenmodes onto this forcing function results in a time-varying function $\xi_n(t) = \int_0^L \Phi_n P(x)\sin(2\pi/\lambda(x - ct))$. Results obtained by integrating for the first four modes are shown in Figure 9.

The integration of the traveling wave forcing function results in oscillating functions that vary successively in phase. This is a possible explanation for the phase shifts in the response functions shown in Figure 8(a). Modes 2 and 3 have the largest amplitude as their wavelengths are closest to that of the selected traveling wave. Using the description of the

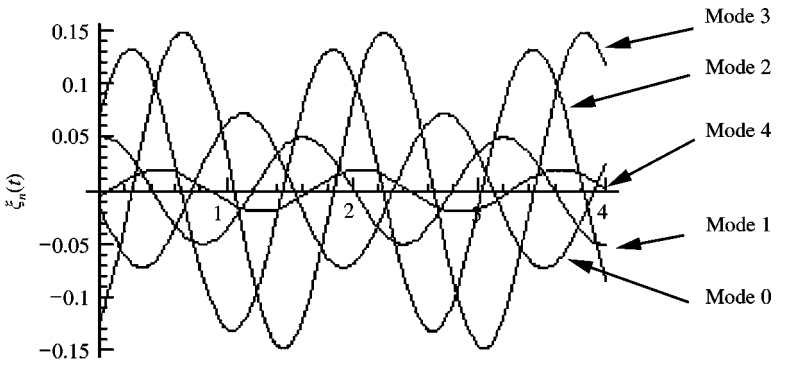

Figure 9. Integration of eigenmodes $\Phi_n(x)$ with $P(x)\sin(2\pi/\lambda(x-ct))$.

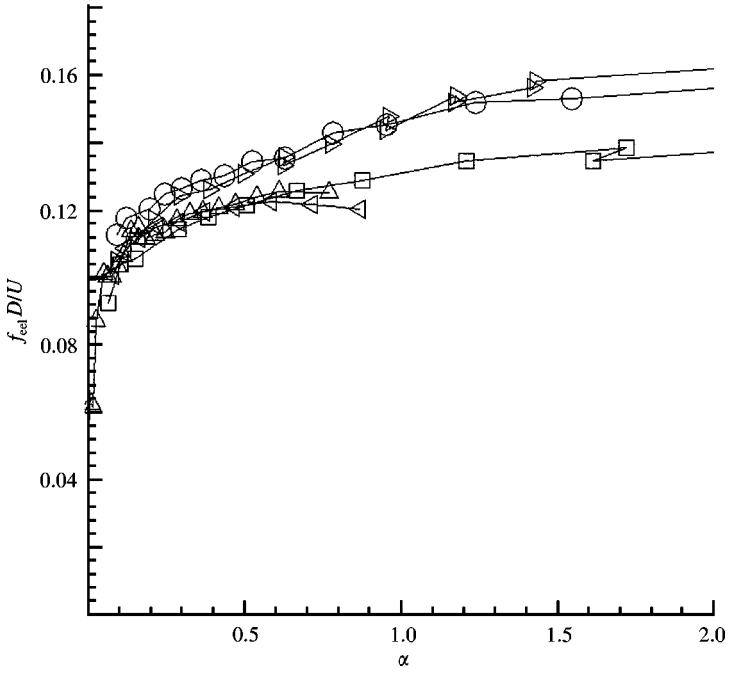

Figure 10. Reduced frequency $f_{eel}D/U_\infty$ versus α: $\triangle$, 18 in PVDF; $\triangleright$, 101 μ in shim stock; $\triangleleft$, 24 in PVDF eel, 1·5 in bluff body; $\bigcirc$, 24 in PVDF, 2 in bluff body; $\square$, map 5.

response of the membrane as $y(x,t)=\sum_{n=1}^{\infty}\Phi_n(x)A_n(t)$, the result of projecting the eigenmodes onto a reduced description of the system gives a system of ordinary differential equations for the time-varying functions $A_n(t)$ as

$$\ddot{A}_n(t)+\omega_n^2A_n(t)=0{\cdot}2U_\infty^2\rho W/\rho_{eel}\xi(t)_n. \tag{3}$$

Solution of these equations for $A_n(t)$ gives similar results to the experimental value of the modal functions. This simplified analysis suggests that the amplitude of response of the respective modes, $\bar{A}_n$, is of order $0{\cdot}2\bar{\xi}_nU_\infty^2\rho W/(\rho_{eel}(-\omega_{eel}^2+\omega_n^2))$, where ω_{eel} is the oscillating frequency of the membrane and fluid, and $\bar{\xi}_n$ is the amplitude of the modal function $\xi_n(t)$. This expression for the modal amplitude term incorporates the effect of the magnitude of

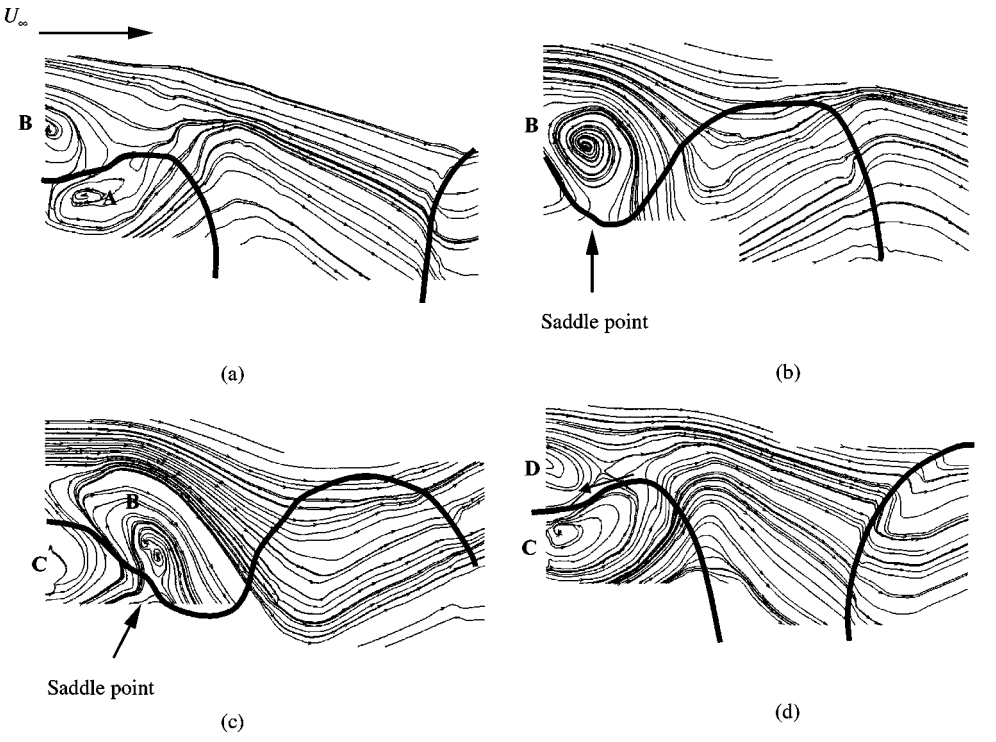

Figure 11. Streamline patterns showing vortex shedding cycle in stationary frame of reference.

the fluid forcing, ρU_∞^2, the forcing frequency ω_{eel}, the mass of the eel, ρ_{eel}, the stiffness of the eel via ω_n and the wavelength of forcing, $\bar{\xi}_n$. We expect that for the eel to be well coupled to the flow, this amplitude should be of the order of the bluff body width; hence, we suggest that when $\alpha = \bar{A}_n/D \approx 1$ the eel should be well coupled to the flow. Figure 10 shows a plot of the response of the nondimensional membrane frequency $f_{\text{eel}}D/U_\infty$ as a function of α. The modal function, $\bar{\xi}_n$, was selected as the function that has the closest wavelength to the structures in the flow. If $\alpha \ll 1$ we expect the membrane to be acting essentially as a long splitter plate and hence poor coupling would be expected, as indicated by a low Strouhal number for $\alpha \approx 0{\cdot}1$. The plot shows that for $\alpha > 1{\cdot}5$ the eel appears to be well coupled, as would be expected if the amplitude of oscillation is larger than the bluff body width. The effect of internal damping and the free stream would be to limit the amplitude of response; these effects are not accounted for in this simplified model of response. The definition of α as the system description parameter follows a similar derivation to the "effective stiffness" parameter defined by Leonard and Roshko (2000).

4. PIV RESULTS

Figure 11 shows the streamline pattern developing around the membrane during one oscillation cycle. The region shown represents about 3/4 of the membrane wavelength. Figure 11(a) shows the presence of two coherent vortical structures, vortex A and B, on the membrane. Vortex A is starting to convect along the underside of the membrane, while vortex B is beginning to impinge on the top surface of the membrane. Both structures show that reversed flow exists on the surface of the membrane close to the pivot point, indicating that secondary vorticity, of opposite sign to the impinging structures, is being generated on

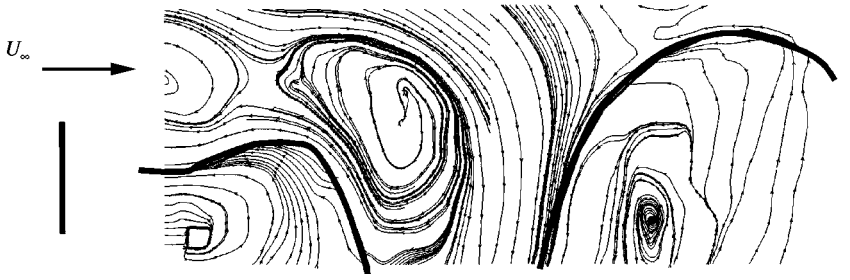

Figure 12. Streamline pattern when moving with bias velocity of $0{\cdot}65U_\infty$.

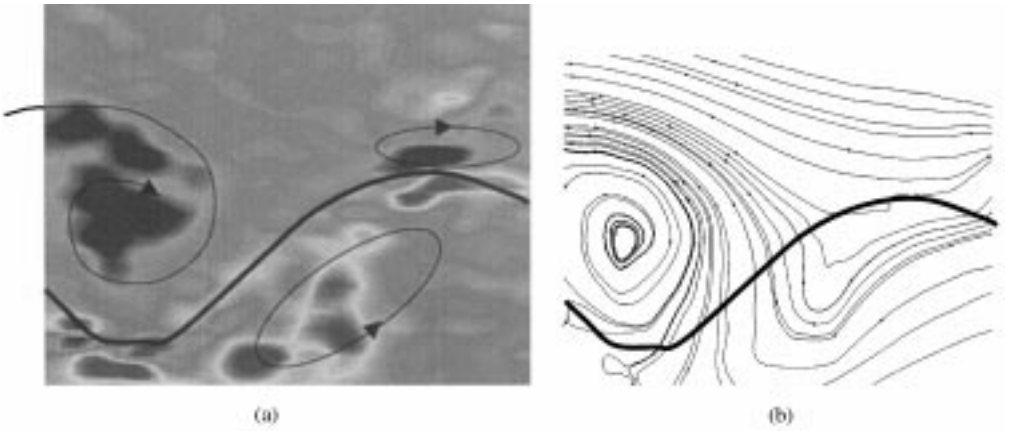

Figure 13. (a) Vorticity field and (b) streamline pattern at the same phase point in shedding cycle.

the membrane surface under these structures. Figure 11(b) shows that the membrane appears to be deforming significantly in response to the impingement of vortex B. The presence of vortex A is no longer evident, although there is significant deformation of the streamline pattern in the region into which it was convecting. In Figure 11(c), vortex B appears to be significantly deforming in response to the membrane, which is now moving upwards as a result of pressure from a newly impinging vortex, vortex C. An interesting feature of Figure 11(c) is the appearance of a saddle point in the flow below the core of vortex B, indicating that two streamlines terminating at the eel surface have joined and bifurcated away from the surface. Figure 11(d), the final phase in the shedding cycle, shows vortex C beginning to convect along the surface and the appearance of a saddle point in the free stream separating the like signed vortical structures, vortex B and D. There is reversed flow under this saddle point and hence a communication of material from vortex B to D. This communication of material has also been observed in flow visualization experiments. The reversed flow is highlighted in Figure 11(d).

Figure 12 shows the streamline pattern for a section of Figure 11(d) when a bias velocity of the order 0.65 of the free-stream velocity has been applied. This velocity bias results in the membrane appearing as a streamline in the flow and also shows the presence of structures along the length of the membrane for the full field of view. This indicates that the vortical structures impinge on the membrane head with significant reversed flow, and then accelerate downstream along the membrane surface. Figure 13 shows a comparison of streamline

and vorticity fields corresponding to the point in the oscillation cycle when an impinging vortex is fully formed and the membrane is at maximum deflection in response to this impinging structure. Vorticity from the previous half of the shedding cycle can be seen on the underside of the membrane.

5. CONCLUSIONS

The response of a flexible membrane or "eel" to external forcing due to the vortex shedding downstream from a bluff body has been examined using frequency response measurements and PIV. Data show that the membranes are able to exhibit lock-in behavior to the bluff body shedding. Lock-in is defined to occur when the membranes oscillate at the same frequency as the undisturbed wake behind the bluff body. When the membrane reaches this condition, its wavelength and amplitude are also similar to the undisturbed vortex street. The amplitude of oscillation appears to be confined to within an envelope that is similar in width to the wake that forms behind the bluff body when no membrane is present. A condition for lock in has been suggested as occurring when $0{\cdot}2\bar{\xi}_n U_\infty^2 \rho W/(\rho_{\mathrm{eel}}(-\omega_{\mathrm{eel}}^2+\omega_n^2)D) > 1$. This relationship is derived from a simplified description of the oscillating system as an Euler–Bernoulli beam and fits the data reasonable well. PIV data sets indicate the presence of vortical structures convecting along the length of the eel according to the wavelength of oscillation. These structures correspond to the alternating vortices that are formed and shed from the edges of the bluff body.

ACKNOWLEDGEMENT

This work is supported by Ocean Power Technologies Inc., Office of Naval Research and DARPA.

REFERENCES

GERRARD, J. H. 1966 The mechanics of the formation region of vortices behind bluff bodies. *Journal of Fluid Mechanics* **25,** 401–413.

HUERRE, P. & MONKEWITZ, P. A. 1990 Local and global instabilities in spatially developing flows. *Annual Review of Fluid Mechanics* **22,** 473–537.

KHALAK, A. & WILLIAMSON, C. H. K. 1999 Motions, forces and mode transitions in vortex-induced vibrations at low mass-damping. *Journal of Fluids and Structures* **19,** 813–851.

LEONARD, A. & ROSHKO, A. 2000 Aspects of flow-induced vibrations. *Journal of Fluids and Structures* **15,** xxx–xxx (this issue).

NAUDASCHER, E & ROCKWELL, D. 1994 *Flow-Induced Vibrations — An Engineering Guide*. Brookfield, VT: A. A. Balkema.

PAIDOUSSIS, M. P. 1966*a* Dynamics of flexible cylinders in axial flow. Part 1. Theory. *Journal of Fluid Mechanics* **26,** 717–736.

PAIDOUSSIS, M. P. 1966*b* Dynamics of flexible cylinders in axial flow. Part 2. Experiments. *Journal of Fluid Mechanics* **26,** 737–752.

ROSHKO, A. 1954 On the drag and shedding frequency of two-dimensional bluff bodies. NACA Technical Note No. 3169.

WU, T. Y. 1961 Swimming of a waving plate. *Journal of Fluid Mechanics* **10,** 321–344.

AUTHOR QUERY FORM

HARCOURT PUBLISHERS

JOURNAL TITLE: JFLS DATE:7/2/2001
ARTICLE NO. : 20000355

Queries and / or remarks

Manuscript Page/line	Details required	Author's response
18/	Leonard & Roshko (2000) Please update	